Solar Physics (2022) 297:112
https://doi.org/10.1007/s11207-022-02049-7

Temporal and Periodic Variations of the Solar Flare Index During the Last Four Solar Cycles and Their Association with Selected Geomagnetic-Activity Parameters

Atila Ozguc[1] · **Ali Kilcik**[2] · **Vasyl Yurchyshyn**[3]

Received: 28 February 2022 / Accepted: 1 August 2022

Abstract
We studied the temporal and periodic variations of the monthly solar flare index (FI) and selected geomagnetic-activity parameters (Ap, Dst, Scalar B, and aa) measured during Solar Cycles 21 – 24 (from January 1, 1975 to December 31, 2020) and report the following findings: 1) all data sets except the FI peak values gradually decreased after 1992, while the FI peak values began their gradual decrease in 1982; 2) all data sets show double or multiple peaks during the maximum phase of solar cycles; 3) the FI shows meaningful correlations with the investigated geomagnetic-activity parameters; 4) the 11-year sunspot-cycle periodicity and periodicities lower than 3.9 months were observed in all data sets without exception; 5) the FI time series exhibits a unique period of 4.8 – 5.2 months that is not present in all the other indices, while geomagnetic aa, Ap, and Dst indices show a unique 6 – 6.1 months periodicity that does not appear in the scalar B and FI; 6) crosswavelet transform (XWT) spectra between FI and other parameters generally show phase mixing in the short (2 – 8 months) period range, while all parameters used in this study were found to be inphase and highly correlated with the 11-year solar-activity period. All these results show that the FI variations are one of the main drivers of the geomagnetic activity.

Keywords Active regions · Flares · Oscillations · Solar · Solar cycle · Observations · Geomagnetic activity

✉ A. Kilcik
alikilcik@akdeniz.edu.tr

A. Ozguc
ozguc@boun.edu.tr

V. Yurchyshyn
vasyl.yurchyshyn@njit.edu

1 Kandilli Observatory and Earthquake Research Institute, Bogazici University, 34684 Istanbul, Turkey

2 Department of Space Science and Technologies, Akdeniz University Faculty of Science, 07058 Antalya, Turkey

3 Big Bear Solar Observatory, New Jersey Institute of Technology, Big Bear City, CA 92314, USA

Published online: 08 September 2022

1. Introduction

Solar activity can be described as a variety of electromagnetic radiations such as low-frequency radio waves as well as powerful gamma-rays, accompanied by particle flux. Among various solar-activity forms, solar flares are known to be one of the strongest and most violent phenomena that are observed. The evolution of solar activity has been studied by numerous researchers, with the aid of long- and short-term solar-activity indicators (Barbieri and Mahmot, 2004; Knaack, Stenflo, and Berdyugina, 2005).

Defined as the Flare Index (FI), the total energy emitted by a flare was described by the formula $FI = it$, which was introduced by Kleczek (1952), in order to estimate the daily flare activity over a 24-hour period. In this formula, i represents the flare intensity measured in the H_α spectral line, whereas t stands for the duration of the flare in minutes. Calculated daily/monthly values are publicly available, provided by the Kandilli Observatory (astronomi.boun.edu.tr/flare-index) as well as by the National Geophysical Data Center (NGDC: www.ngdc.noaa.gov/stp/solar/solarflares.html). Flare-activity reviews utilizing the flare index are given for each day from 1936 to 2001 by Kleczek (1952), Knoska and Petrasek (1984), Atac and Ozguc (1998), and Atac and Ozguc (2001). The flaring-activity signatures in magnetic regions could be identified commonly by using FI. In order to differentiate between flaring and nonflaring regions, FI was utilized to test the efficiency of measurements of the topological complexity of the magnetic-field concentrations (Ermolli et al., 2014, and references therein). By using FI and magnetic-power spectra, Abramenko (2005) and Abramenko and Yurchyshyn (2010) detected flare-productive active regions.

Solar-output variations are well known to be within approximately 27-day and 11-year periods; the former related to the modulation imposed by the rotation of the Sun and the latter reflecting the sunspot cycle. It is of the outmost importance to detect and calculate the statistical significance of flare periodicities, for the benefit of the study of the physical properties of the Sun. Within the extreme time scales of 27 days and 11 years, following the discovery of a 153-day periodicity (Rieger et al., 1984), the midrange periods (Bai, 2003), and periodicities within this range have been extensively studied (Ichimoto et al., 1985; Dennis, 1985; Bai and Sturrock, 1987; Ozguc and Atac, 1989; Droege et al., 1990; Verma et al., 1991; Kile and Cliver, 1991; Vaquero, Gallego, and Trigo, 2007; Kilcik et al., 2010; Chowdhury et al., 2016; Ozguc et al., 2021).

Many solar studies considered solar flares as one of the most important solar events affecting the Earth, along with coronal mass ejections (CMEs) (Kilcik et al., 2011, and references therein). When a strong solar event occurs on the Sun, a stream of high-speed particles that is released along with strong magnetic fields ejected from the solar corona may have a significant impact on the near-Earth space environment. Such an impact is called a geomagnetic storm and it may affect the Earth in many different ways including satellite drag, communication cut-off, power-grid failures, etc. Disturbances of the near-Earth environment are measured and monitored by means of various geomagnetic parameters, such as aa (Mayaud, 1972), Ap (Bartels, Heck, and Johnston, 1939), and Dst (Sugiura, 1964) indices, which show some level of a relationship with solar activity and this relationship has been extensively studied in the past (Echer et al., 2004; Verbanac et al., 2011; Du, 2015; Kirov et al., 2018). Periodic variations of solar activity and the related effects in the terrestrial environment have been studied for a long time and cotemporal periodicities between different solar- and geomagnetic-activity parameters have been reported (Cadavid et al., 2005; Kilcik et al., 2020; Ozguc et al., 2021). However, contradictory results such as phase mixing, nonexistence of some periodicities, etc. still remain.

In this study we focus on the comparison of the temporal and periodic variations detected in the solar FI and selected geomagnetic-activity indices measured during the last four Solar

Cycles (21 – 24). Their relationships are described by means of time profiles, correlations, and periodicity analyses. We describe the data and methods used in Section 2, the analysis and results are given in Section 3, and the discussion and conclusions are given in Section 4.

2. Data and Methods

We compared monthly averaged FI data with selected monthly averaged geomagnetic-activity parameters for Cycles 21 to 24 (from 1976 to 2019). All monthly values are calculated by taking the average of the daily values over the months. The geomagnetic-activity parameters selected are as follows:

(1) The aa index is a simple global geomagnetic-activity index introduced by Mayaud (1972). It is derived from the K indices from two approximately antipodal observatories located at $\pm 50^{\circ}$ latitude (Hartland in the United Kingdom and Camberra in Australia) and it measures the amplitude of global geomagnetic activity during 3-hour intervals. This is the geomagnetic index with the longest available record, with data since 1868.

(2) The Disturbance Storm Time (Dst) index was proposed by Sugiura (1964) to measure the magnitude of magnetospheric currents that produce an axially symmetric disturbance field. This index is a measure of the variation of the field due to the ring current arising in the magnetosphere during a geomagnetic storm. Data from four observatories are used to derive the Dst index. Because of the need for good data, these observatories were chosen sufficiently far from the auroral and equatorial electrojet regions. Irregularities observed in the Dst index that have a negative sign and fluctuate within the -50 nT $\leq$ Dst < -30 nT range are called small storms, while those within the -100 nT $\leq$ Dst < -50 nT range are called moderate storms, -200 nT $\leq$ Dst < -100 nT fluctuations are called intense storms, and a Dst index below -250 nT defines big geomagnetic storms (Gonzalez, Tsurutani, and Clúa de Gonzalez, 1999).

(3) Ap index: the K index is used to measure changes in the horizontal component of the magnetic field. However, since the K index is not directly related to geomagnetic activity the Kp index was introduced and it is derived from the mean standardized K index of 13 geomagnetic observatories located between ± 44 and 60 degrees of the geomagnetic latitude. This planetary index is designed to measure the magnetic effect of solar particle radiation. The 3-hourly ap index is derived from the Kp index and the Ap index used in this study is an average of the ap index over 24 hours (Bartels, Heck, and Johnston, 1939).

(4) The interplanetary magnetic field (IMF) includes solar magnetic fields that were carried into interplanetary space by the solar wind. The source of the fast solar wind is thought to be coronal holes, which are open magnetic-field regions on the Sun, while slow solar wind originates at closed magnetic regions thought to be associated with active regions. The structure and dynamics of the IMF (scalar B) are key for understanding space weather (Owens and Forsyth, 2013).

All geomagnetic-activity parameters, except the aa index, were taken from the OMNIWeb data base (omniweb.gsfc.nasa.gov). The aa index data are available at the International Service of Geomagnetic Indices data base (ISGI: isgi.unistra.fr). We have calculated average monthly values of these indices for the 1975 – 2020 time interval, and used them in this study.

To investigate the relationship between FI and the selected geomagnetic parameters we first produced plots of their time variations. Then, the crosscorrelation analysis was performed and highest correlation coefficients between FI and the indices were obtained along with the corresponding time lags.

To examine details of periodic variations of each monthly time series we used the Multi Taper Method (MTM) and Morlet wavelet analysis methods. The MTM provides useful tools for spectral estimation (Thomson, 1982; Percival and Walden, 1993) and signal reconstruction (Park, 1992) of a time series whose spectrum may contain both broadband and line components. More details about this method can be found in Ghil et al. (2002). This method has been successfully applied to the analysis of various data sets (Ghil et al., 2002; Fang et al., 2012; Escudier, Mignot, and Swingedouw, 2013; Kilcik et al., 2018; Chowdhury et al., 2019; Kilcik et al., 2020, and references therein). Here, we used three sinusoidal tapers and the frequency range was chosen between 0.004 and 0.5 (2 – 205 months). The significance tests were carried out assuming that the noise has a red spectrum. We consider that a signal is detected when the 95% confidence level is reached. To obtain the localization of the above periodicities we used the Morlet wavelet method (Torrence and Compo, 1998) that has been utilized in many solar studies (Chowdhury et al., 2019; Oloketuyi, Liu, and Zhao, 2019; Kilcik et al., 2020, and references therein). In this study, the FI, Ap, Dst, Scalar B (IMF), and aa indices were analyzed using the biwavelet package written in R programming language (github.com/tgouhier/biwavelet). A "Morlet" mother function was used considering the "red noise" background with a nondimensional frequency (Torrence and Compo, 1998). The effect of edges is represented by the cone of influence (COI).

We also used "crosswavelet transform" (XWT) and "wavelet coherence" (WTC) methods that are also part of the biwavelet package. These two methods were also used by various authors (Poluianov and Usoskin, 2014; Xiang and Kong, 2015; Chowdhury et al., 2019; Kilcik et al., 2020; Mares et al., 2021). They allow us to infer a nonlinear relationship and common periods between two analyzed data sets, X and Y. The XWT spectrum shows the phase relationship that is represented by arrows with the following convention: pointing right, inphase; pointing left, antiphase; pointing straight up, the second series Y leads by 90°; pointing straight down, the first series X leads by 90°. The case when the arrows are distributed randomly indicates phase mixing between X and Y. The WTC spectrum indicates the amount of common power between two time series as a function of time and frequency by computing the crosscorrelation between the two time series (Maraun and Kurths, 2004; Grinsted, Moore, and Jevrejeva, 2004; Chang and Glover, 2010; Chowdhury et al., 2019). Here, we compared the total FI data with each of the other indices used in this study.

3. Analysis and Results

3.1. Temporal Variation and Correlation Analyses

Figure 1 shows the temporal variation of all parameters used in this study during the 1975 – 2020 time interval.

As shown in Figure 1 all geomagnetic-activity indices have the highest peak amplitude during the maximum phase of Solar Cycle 22, while the FI data have the maximum peak amplitude during Solar Cycle 21. When we consider the temporal variation of each parameter separately the following results are obtained: i) the scalar B, Ap, Dst, and aa indices have their highest amplitude during the maximum phase of Solar Cycle 22, then they start to decrease gradually during the maximum phases of the following solar cycles with double/multiple peak structures; ii) unlike geomagnetic indices, the highest amplitude of the FI data increased from Solar Cycles 21 to 22, after which it began to decrease gradually similarly to the geomagnetic indices. Note that the FI profiles also show double/multiple peak structures during the maximum phases of all investigated solar cycles. These results show

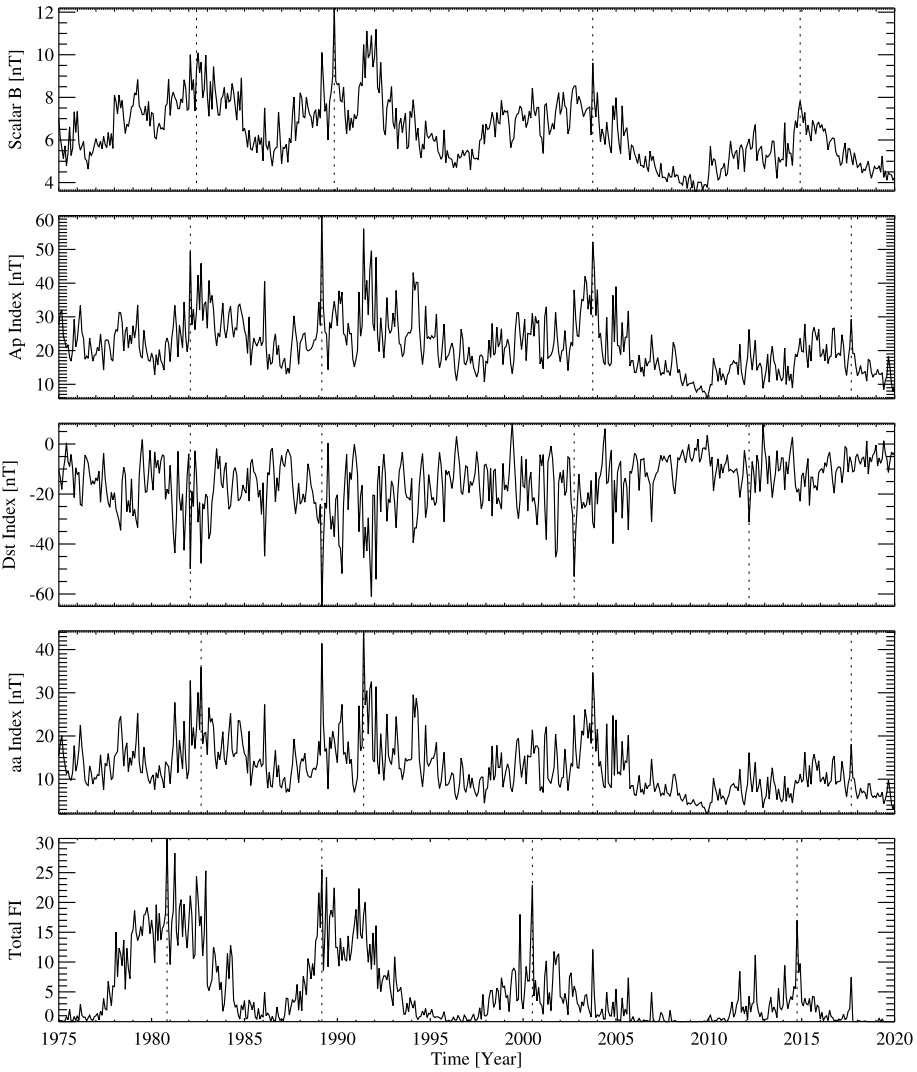

Figure 1 Temporal variations of investigated parameters for the time period of 1975 – 2020. The vertical dashed lines represent the peak position of each parameter for each cycle.

that solar flares are not the only drivers of geomagnetic activity and other solar-activity events such as CMEs, solar winds, etc. also have a strong effect on the temporal variation of the geomagnetic activity. Table 1 lists the monthly mean values of the maximum amplitudes of all parameters for the investigated solar cycles. From this table the peak values of the FI decreased about 17%, 10%, and 26% from Cycles 21 to 22, 22 to 23, and 23 to 24, respectively. All other indices increased more than 20% from Cycle 21 to 22 and then start to decrease gradually; the Ap, Dst, aa, and scalar B decreased about 13%, 18%, 22%, and 21% from Cycle 22 to 23, respectively. The decrease continued from Cycle 23 to 24 as about 44%, 41%, 48%, and 19% for the same parameters, respectively.

Table 1 The maximum amplitudes of all used parameters for the investigated solar cycles.

Data	Cycle 21	Cycle 22	Cycle 23	Cycle 24
FI Index	30.73	25.53	22.94	17.01
Ap Index	49.35	60.04	52.24	29.27
Dst Index	−49.96	−64.97	−53.00	−31.19
aa Index	35.93	44.33	34.68	18.07
Scalar B	10.09	12.20	9.62	7.80

Table 2 Correlation coefficients and time lags between the monthly FI and geomagnetic-activity parameters.

Data	aa Index		Dst Index		Ap Index		Scalar B	
	Correlation coefficient	Lag [Month]	Correlation coefficient	Lag [Month]	Correlation coefficient	Lag [Month]	Correlation coefficient	Lag [Month]
Flare index	0.47 ± 0.07	27	-0.45 ± 0.07	0	0.51 ± 0.06	0	0.70 ± 0.05	0

Figure 2 and Table 2 show results of the crosscorrelation analysis with the corresponding time lags. The crosscorrelation analysis gives the highest correlation coefficients between two analyzed time series with possible time lags. In this method, zero time lag means that there is no time lag between the two time series, while a positive time lag means the first parameter (here FI) leads the second (geomagnetic-activity indices) and vice versa. As shown in Figure 1, the FI data reached its maximum about two years before the aa index. We found that FI data show the highest correlation with scalar B ($r = 0.69 \pm 0.05$) and the lowest correlation with the Dst index ($r = -0.45 \pm 0.07$). Contrary to other parameters, only the geomagnetic aa index shows a 27-month time lag with the FI data. As shown in Figure 1, all geomagnetic-activity indices reach their maxima/minima during the same time of the investigated time period. This result shows that the differences in the time delays and correlation coefficients are due to the small-scale variations in the data sets.

3.2. Periodicity Analysis

Figures 3 to 7 show the results of the MTM and Morlet wavelet analyses of the data sets. Note that all wavelet analyses were carried out with 95% confidence level of red-noise approximation and the black contours in the wavelet scalograms show the localization of meaningful periodicities with at least 95% confidence level. The red colors in the color bars (located at the right side of the wavelet scalograms) show the placement and existence of meaningful periods, while the blue colors indicate the nonexistence of meaningful periods. The MTM analysis provides frequency, power, 95%, and 99% confidence levels of all frequencies under the red-/white-noise approximation. Here, all period analyses were carried out with the red-noise approximation. After obtaining all these parameters, we manually filtered all meaningful periods and their lowest significance levels for each data set and the obtained results are shown in Table 2. To show the MTM plots more clearly, the MTM powers and significance levels were normalized to the values of the 95% confidence level.

From Table 3 and the above figures we would like to underline the following results: 1) in all data sets we detected the 11-year sunspot-cycle periodicity as well as periodicities lower than 3.9 months; 2) the FI data have one unique interval of periods (4.8 – 5.2 months) that

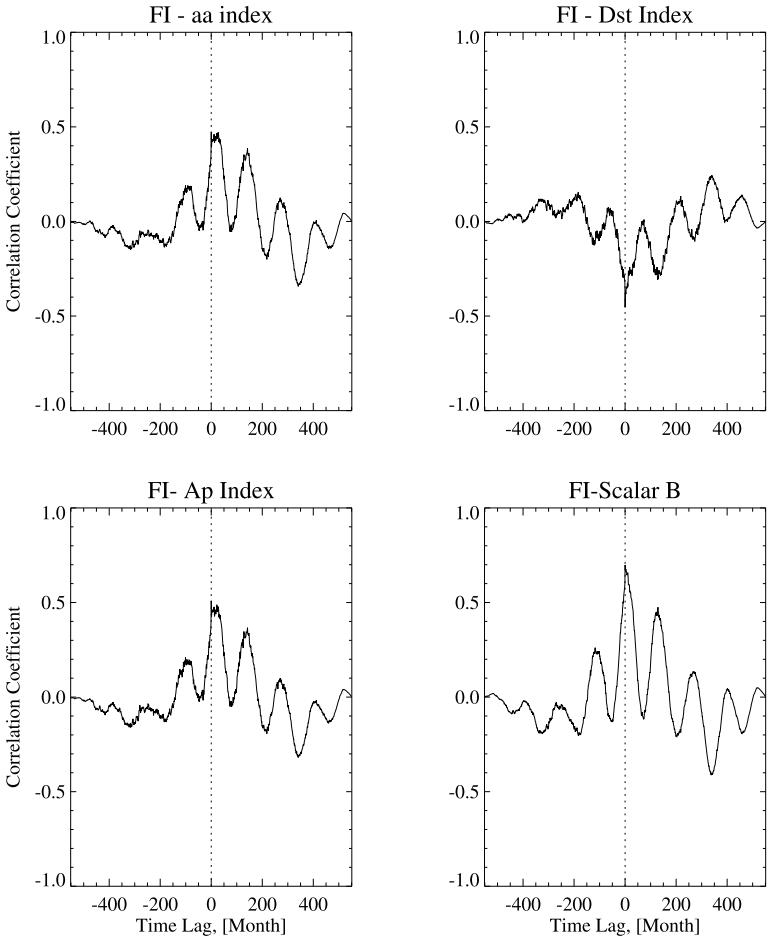

Figure 2 Crosscorrelation analysis results for the investigated parameters. The vertical dotted lines show the zero-time lag.

is not present in all other time series; 3) geomagnetic aa, Ap, and Dst indices show 6 – 6.1 month periodicity and this period is not present in the scalar B and FI; 4) only geomagnetic aa and Ap indices show the same periodic variations with almost the same confidence levels; 5) only a few well-pronounced periodicities were observed during Solar Cycle 24, and they were the most prominent during the maximum phases of the investigated solar cycles. About one month solar-rotation periodicity appears in FI and scalar B data sets (see Figures 3 and 7), about 3 months periodicity appears in the Dst index and scalar B time series (see Figures 6 and 7) during the maximum phase of Solar Cycle 24. From the wavelet scalograms, we can see that the spectral power of all data sets decreased drastically during Solar Cycle 24. A possible reason for this is the weak solar activity and, in particular, the low solar-flare activity. It is clear that the decrease in solar activity will result in a decrease in geomagnetic activity, and therefore the spectral power of the geomagnetic-activity indices weakened during the same period.

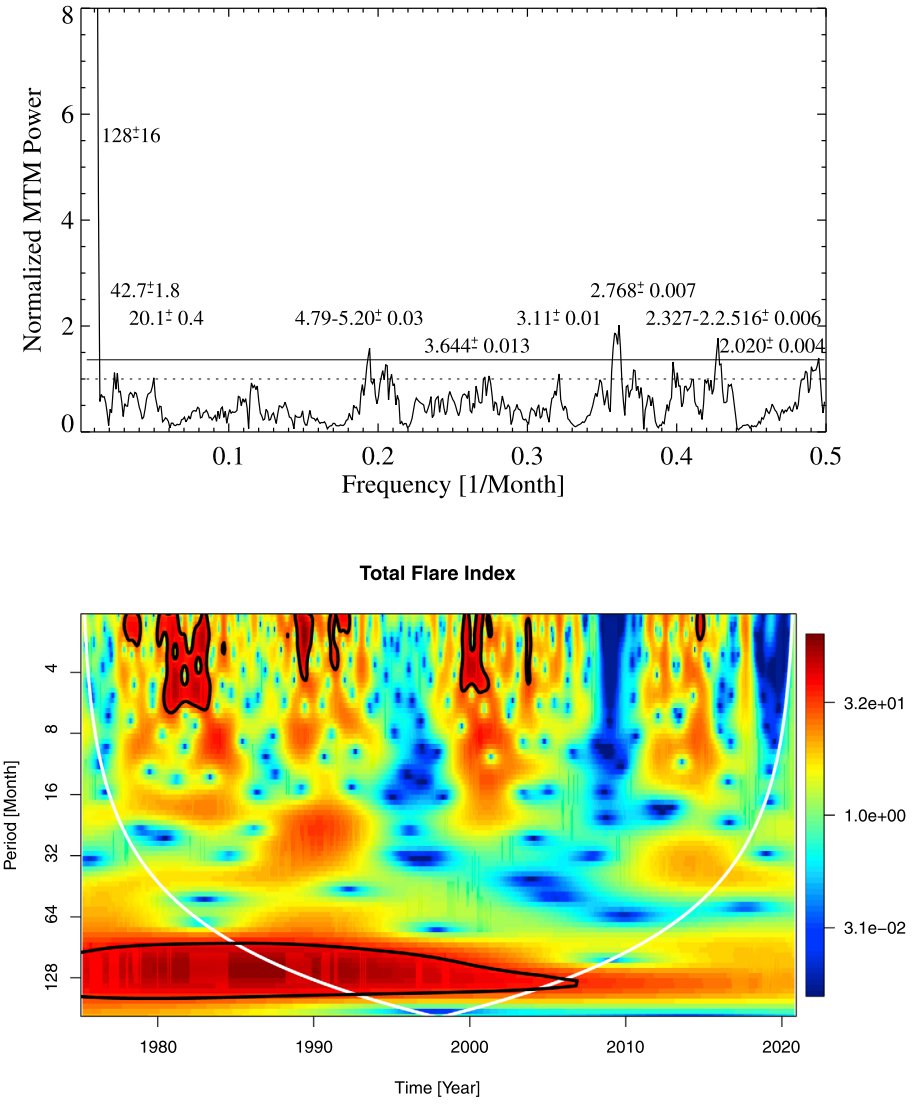

Figure 3 Results from MTM (upper panel) and Morlet wavelet (lower panel) analyses applied to FI data. Dotted and dashed lines in the MTM spectrum represent 95% and 99% confidence levels, and the white line in the Morlet wavelet spectrum describes the cone of influence.

We also compared results from the FI Morlet wavelet analysis with the other parameters by the XWT and CWT analysis (Figures 8, 9, 10, and 11). In this way we could obtain correlations and phase relationships (black arrows in figures) between FI and all other parameters. Some of the arrows are located outside the region delimited by the black boundaries due to the limitation of the plotting routine. The arrows show that there are periodicities but with significance just below the 95% confidence level. Here, we only focused on the correlation and phase relationship of the meaningful periodicities.

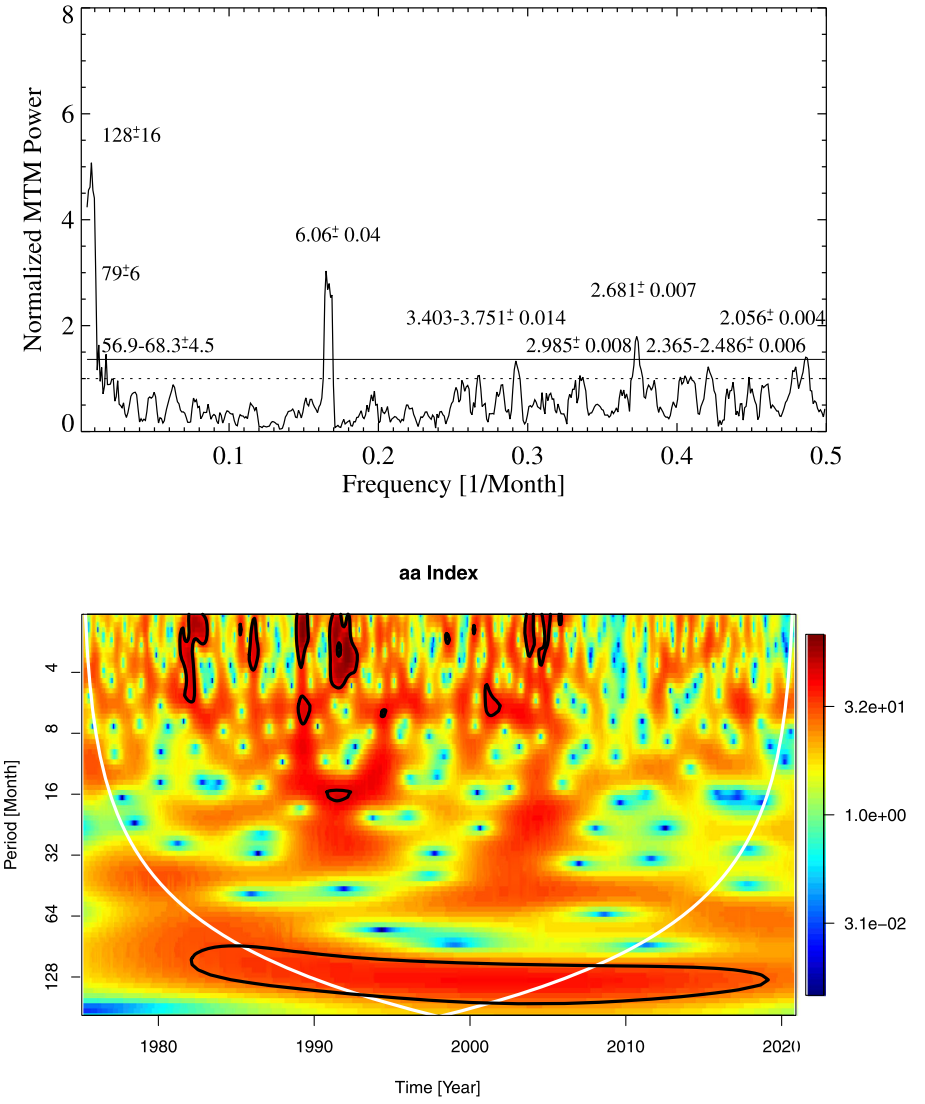

Figure 4 Results from MTM (upper panel) and Morlet wavelet (lower panel) analyses applied to the aa-index data. Dotted and dashed lines in the MTM spectrum represent 95% and 99% confidence levels, and the white line in the Morlet wavelet spectrum describes the cone of influence.

As mentioned previously, the XWT and WTC analyses showed the correlation and phase relation of wavelet analysis of the two data sets compared (FI and other parameters). In these plots the warmer colors (red) represent regions with significant interrelation, while colder ones (blue) signify a lower dependence between the series. From the XWT and WTC plots in Figures 8, 9, 10, 11 we extract the following results; I) FI and the other parameters here analyzed display evidence of significant periods where the periodicities of FI and other parameters (aa, Ap, Dst, and scalar B) are correlated in time (see black contours and red

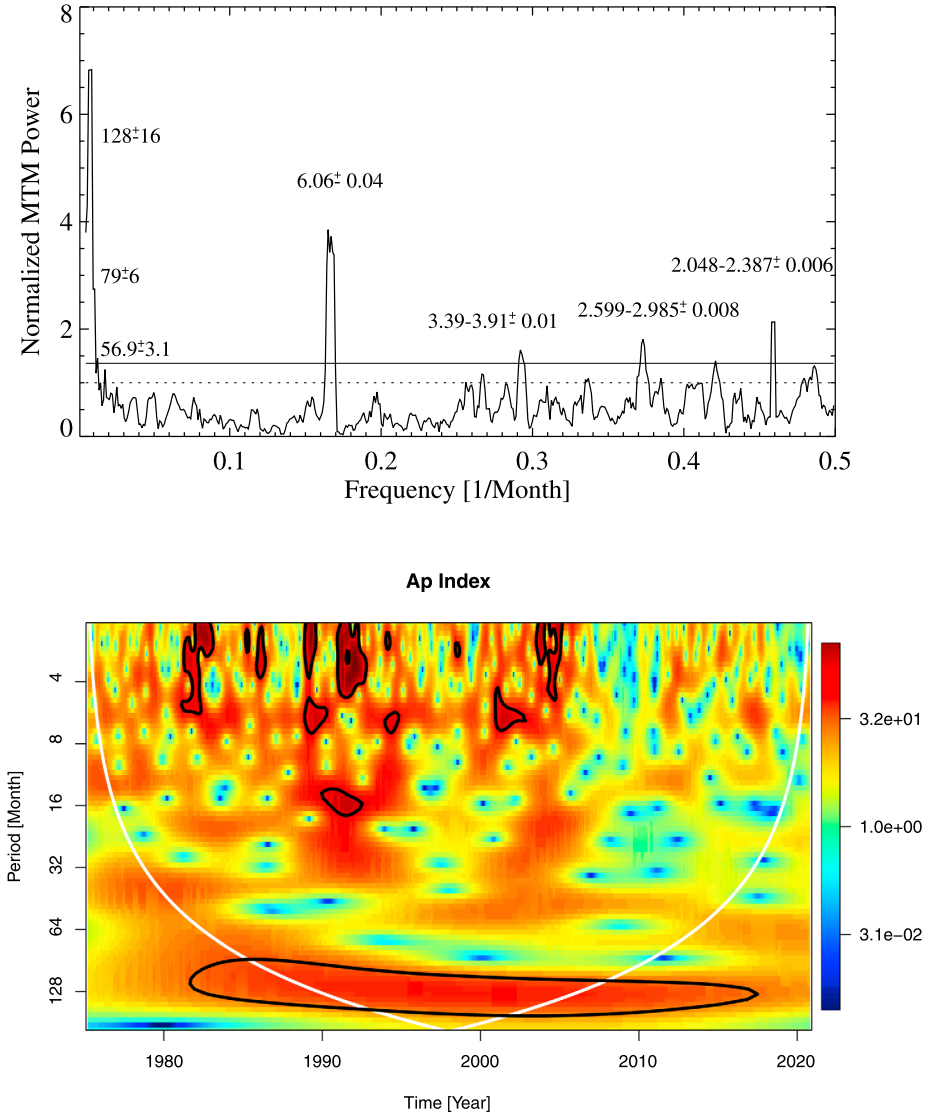

Figure 5 Results from MTM (upper panel) and Morlet wavelet (lower panel) analyses applied to the Ap index data. Dotted and dashed lines in the MTM spectrum represent 95% and 99% confidence levels, and the white line in the Morlet wavelet spectrum describes the cone of influence.

colors in XWT and WTC plots). For example, the 11-year periodicity in the XWT plot of Figures 8 – 11 shows strong correlations. II) The XWT spectra between FI and other parameters generally show phase mixing for periods between 2 to 8 months, since the directions of arrows are mixed. For example, it can be seen from the same figures that the direction of arrows are mixed around 1990 between FI and other indices. Contrary to small periods, all parameters used in this study are inphase and highly correlated for the 11-year Solar Cycle periodicity. Note that FI and Dst index data are in antiphase due to the negative sign of Dst values for the same periodicity. III) Correlations for all data sets at small periods (0 – 8

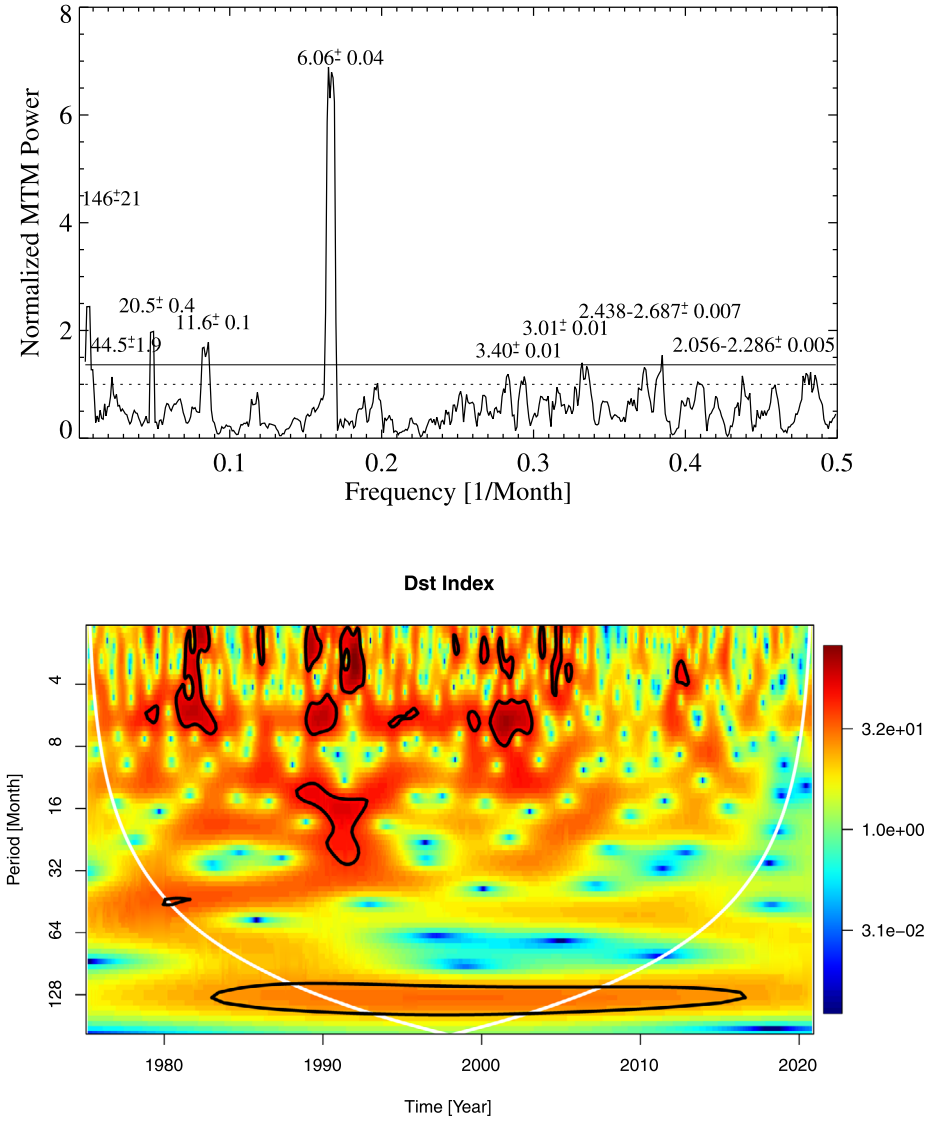

Figure 6 Results from MTM (upper panel) and Morlet wavelet (lower panel) analyses applied to the Dst index data. Dotted and dashed lines in the MTM spectrum represent 95% and 99% confidence levels, and the white line in the Morlet wavelet spectrum describes the cone of influence.

months) decreased for the investigated time period except for the declining phase of Solar Cycle 23 (see extensions and number of black contours in WTC plots). IV) As shown in the lower panels of Figures 8 – 11, there are many black contours between 8 to 45 months. This indicates the existence of similar periodicities between the compared parameters and thus correlations are more pronounced.

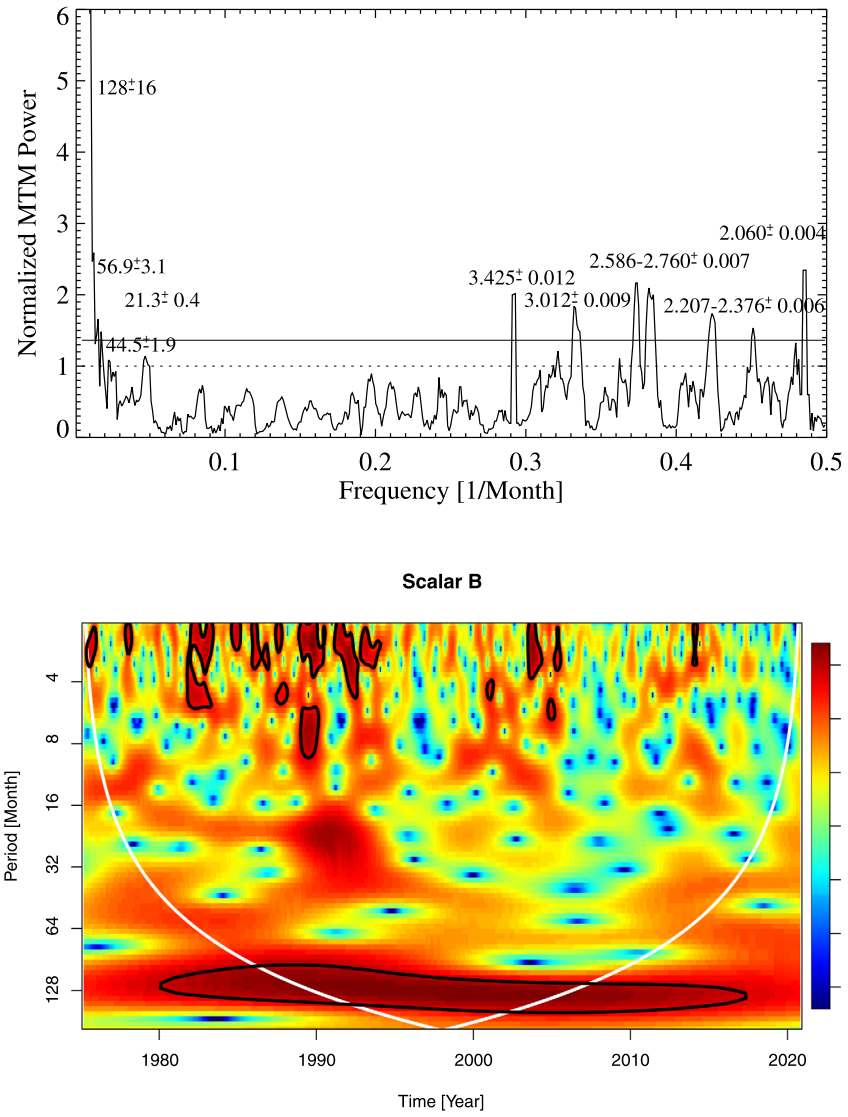

Figure 7 Results from MTM (upper panel) and Morlet wavelet (lower panel) analyses applied to the scalar B data. Dotted and dashed lines in the MTM spectrum represent 95% and 99% confidence levels, and the white line in the Morlet wavelet spectrum describes the cone of influence.

4. Discussion

4.1. Temporal-Variation Analysis

Kakad et al. (2019) compared the relative decrease in the peak sunspot number of consecutive solar cycles for Cycles 21 to 24 and found that the decrease amounted to 8.7%, 15%, and 35% for Cycles 22, 23, and 24, respectively. Carrasco et al. (2016) analyzed sunspot-area time series starting in 1832 and found that the peak value of sunspot area was slightly

Table 3 Periods detected by making use of the MTM analysis and their significance level.

Period (Month)	FI	aa Index (nT)	Ap Index (nT)	Dst Index (nT)	Scalar B (nT)
114 – 128	+ > 99%	+ > 99%	+ > 99%	+ > 99%	+ > 99%
78 – 79	–	+ > 99%	+ > 99%	–	–
57 – 68	–	+ > 99%	+ > 95%	–	+ > 99%
42 – 45	+ > 95%	–	–	+ > 99%	+ > 99%
20 – 22	+ > 95%	–	–	+ > 99%	+ > 95%
6.0 – 6.1	–	+ > 99%	+ > 99%	+ > 99%	–
4.8 – 5.2	+ > 95%	–	–	–	–
3.3 – 3.9	+ > 95%	+ > 95%	+ > 95%	+ > 95%	+ > 99%
2.5 – 3.1	+ > 95%	+ > 95%	+ > 95%	+ > 95%	+ > 99%
2.2 – 2.4	+ > 99%	+ > 95%	+ > 95%	+ > 95%	+ > 99%
2.0 – 2.19	+ > 95%	+ > 95%	+ > 95%	+ > 95%	+ > 99%

higher during Solar Cycle 22 in comparison to Solar Cycle 21. Here, we analyzed the solar FI, and some geomagnetic-activity parameters (scalar B, aa, Ap, and Dst) for the last four Solar Cycles (from Cycle 21 to 24) and found that all parameters' peak values were higher during Solar Cycle 22 compared to Cycle 21, except the FI. The FI peak value gradually decreased from the maximum of Solar Cycle 21 to 24 (see Table 1). Thus, we may conclude that the solar FI follows the sunspot-number (SSN) time series while other indices used in this study follow the sunspot-area (SSA) time series. Also, we may speculate that to describe the geomagnetic activity, the SSA time series might be more useful in comparison to the SSN or FI data.

Many solar indices (e.g., SSN, SSA, $F_{10.7}$ solar radio flux, FI, etc.) exhibit 11-year periodic variations with a plethora of fine-scale temporal structures. The most prominent feature is the fine structure of the solar maximum, when two or more peaks can be clearly identified in time profiles. The double-peaked solar maximum was first identified using observations with the green coronal line (Gnevyshev, 1967, 1977) and it is commonly known as the "Gnevyshev gap". The gap is also observed in various data sets acquired in all layers of the solar atmosphere (photosphere, chromosphere, and corona) and in a wide spectral range (visible and radio) and it is expected to be associated with the heliomagnetic cycle (e.g., Feminella and Storini, 1997). The Earth's magnetosphere directly responds to this solar-activity feature and the double-peak structure was also detected in magnetospheric data (Gonzalez, Gonzalez, and Tsurutani, 1990; Storini et al., 2003; Echer et al., 2004). Thus, Ahluwalia (2000) suggested that the solar polar-field reversal may give origin to the Gnevyshev gap seen in the Ap index. Kane (2010) reported the double-peak structure during the rising phase of Solar Cycle 23 analyzing sunspot numbers, Ly-α data, 2800 MHz solar radio emission $F_{10.7}$, the coronal index, the mean magnetic field as well as the geomagnetic indices Dst, Ap, AU, AL, and AE. Ozguc et al. (2021) reported that Solar Cycle 24, similarly to the previous Cycle 23, is also double peaked. Takalo (2021) analyzed the OMNI2 data for 1964 – 2020 (from Cycles 20 to 24) and found that the gaps are also present in the solar-wind velocity and the IMF intensity (scalar B). In this study, we further confirm the above findings and report that the double/multiple peaks were detected in the geomagnetic-activity indices measured for the last four solar cycles.

Kilpua et al. (2014) analyzed Dst, Auroral Electrojets (AE), and interplanetary magnetic field (Scalar B) during the 1995 – 1999 and 2006 – 2012 periods and found very low ge-

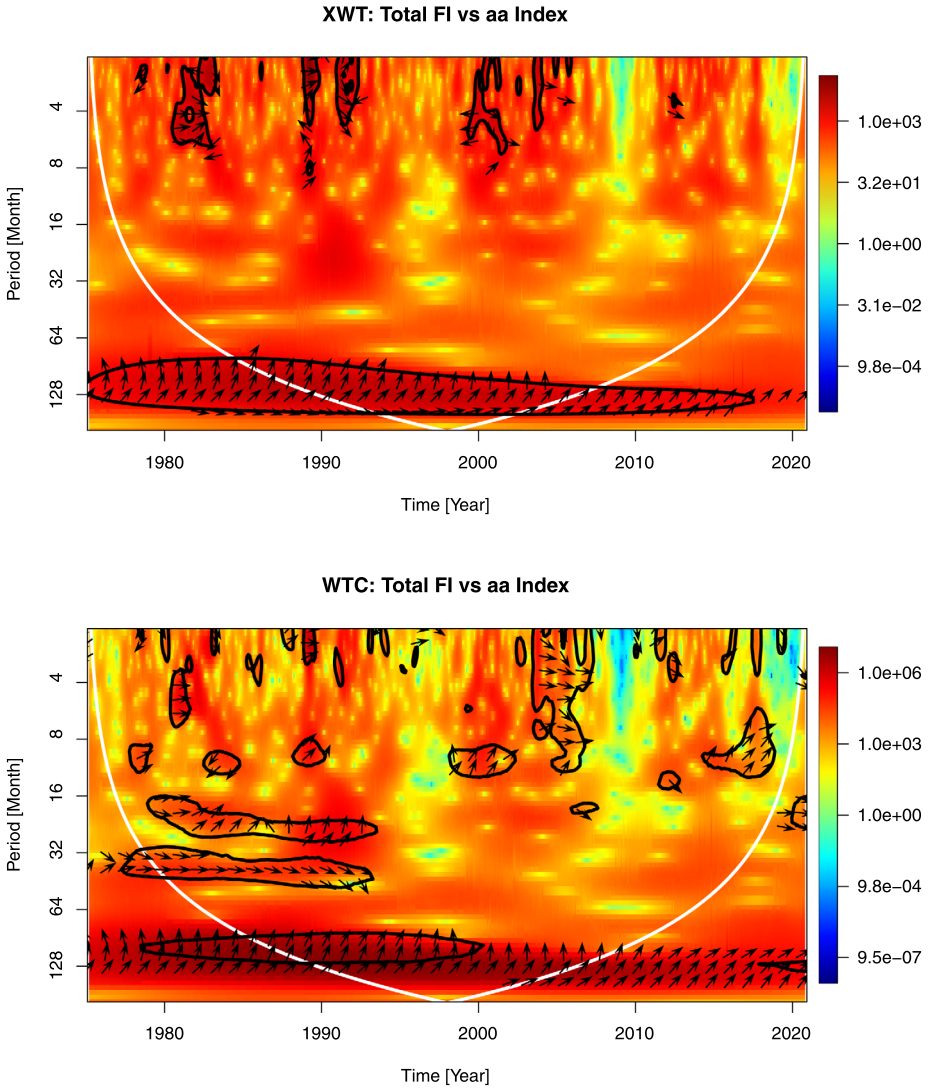

Figure 8 XWT (upper panel) and WTC (lower panel) spectrum between monthly FI and aa index.

omagnetic activity during Solar Cycle 24. This result shows a good agreement with our findings. Kilcik et al. (2017) found high correlations ($r = 0.62$, $r = -0.44$) between Ap and Dst indices and with sunspot counts of large active regions. Verbanac et al. (2011) compared annual Ap and Dst indices with 10.7 cm solar radio flux, SSN, SSA, and group SSN and found meaningful correlations between these parameters and the Dst index with a zero-time lag, and one or two years time lag with the Ap index. Here, we compared monthly FI with aa, Ap, Dst, and scalar B and found meaningful correlations ($r = 0.47$, $r = -0.45$, $r = 0.51$, and $r = 0.7$ for aa, Dst, Ap, and scalar B, respectively) with a zero-time lag, except for the aa index that shows about a two-year time lag with the FI data. Thus, we may conclude that the solar FI is closely related to geomagnetic activity and especially with the IMF.

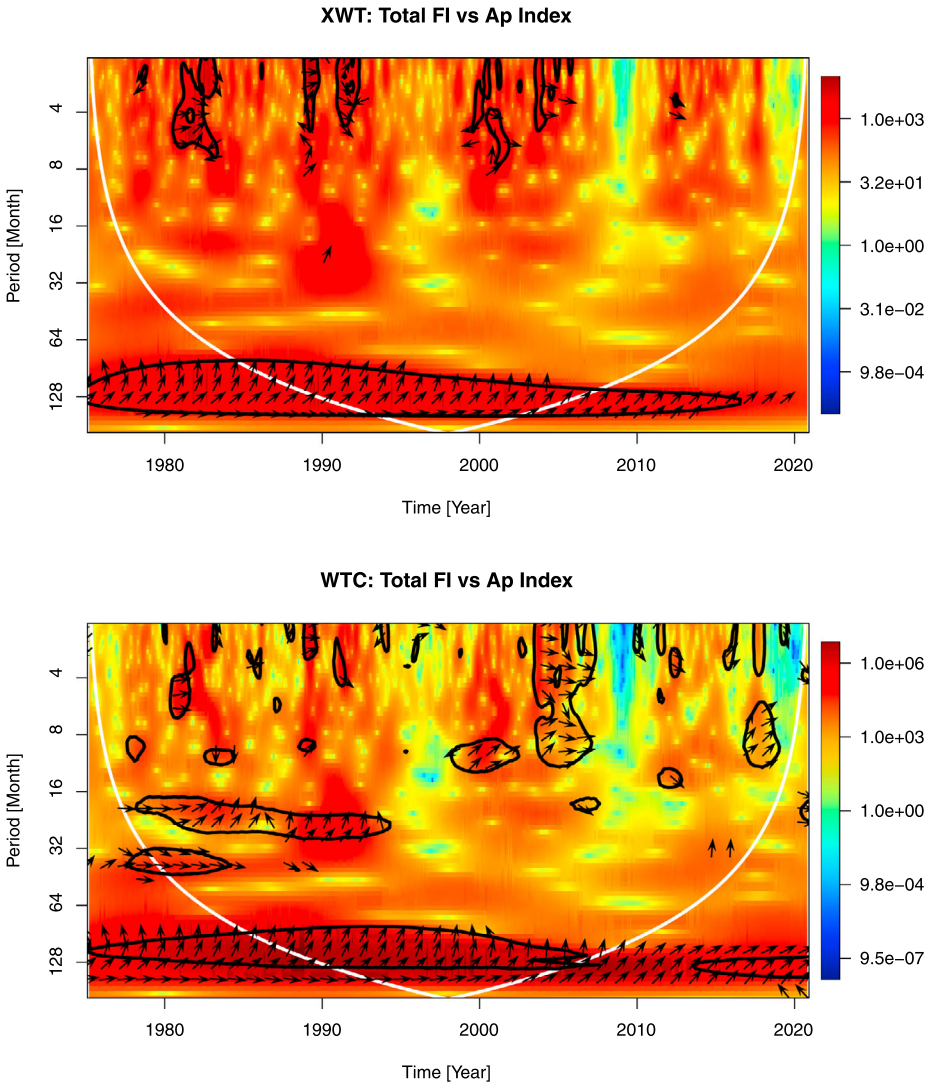

Figure 9 XWT (upper panel) and WTC (lower panel) spectrum between FI and Ap index.

4.2. Periodicity Analysis

Singh and Badruddin (2014) applied Morlet wavelet and global wavelet analysis tools to SSN and aa index time series and reported 27.8-, 157-, and 370-day, and 2.2-, 5.5-, 11-, 22.7-, and 38.6-year periods for the SSN data and 13.8-, 26.6-, and 185-day, and 5.3-, 11-, 30-, and 46-year periods for the aa index. They argued that the 27-day, 5.3-year, and 11-year periodicities found in the aa index have a solar origin. Further, Chowdhury et al. (2015) reported 20 – 35-, 45 – 60-, 100 – 130-, 140 – 170-, and 180 – 240-day periodicities, while Marques de Souza Franco et al. (2021) analyzed monthly 10.7 cm solar radio flux and geomagnetic ap and Dst indices for over five solar cycles (1963 – 2019) and found a 0.5-year periodicity in both Ap and Dst indices.

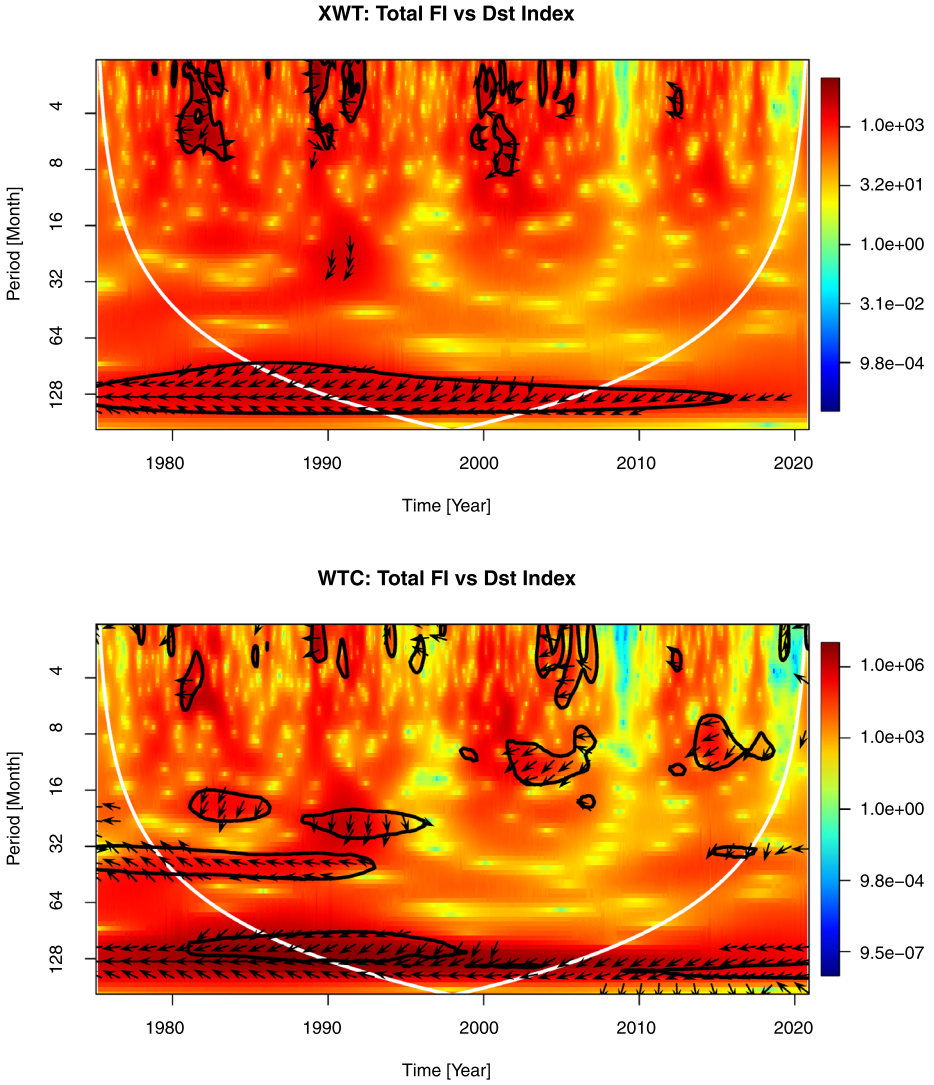

Figure 10 XWT (upper panel) and WTC (lower panel) spectrum between FI and Dst index.

In our study, we investigated the periodicities of solar FI, and geomagnetic-activity parameters (scalar B, aa, Ap, and Dst) by using MTM and Morlet wavelet analysis methods and confirm most of the above results. We obtained about 11-year solar-cycle periodicities in all data sets without any exception. For about 5.5 – 5.3-year periodicity found by Singh and Badruddin (2014) from both SSN (5.5 year) and aa index (5.3 year), we found the same periodicity in aa and Ap indices, but contrary to their results we could not detect this periodicity in our MTM analysis at the 95% confidence level in the solar FI and geomagnetic Dst index data sets. Thus, we may speculate that this periodicity may not be of solar origin, or it is not related to solar-flaring activity. For the semiannual periodicity found by Marques de

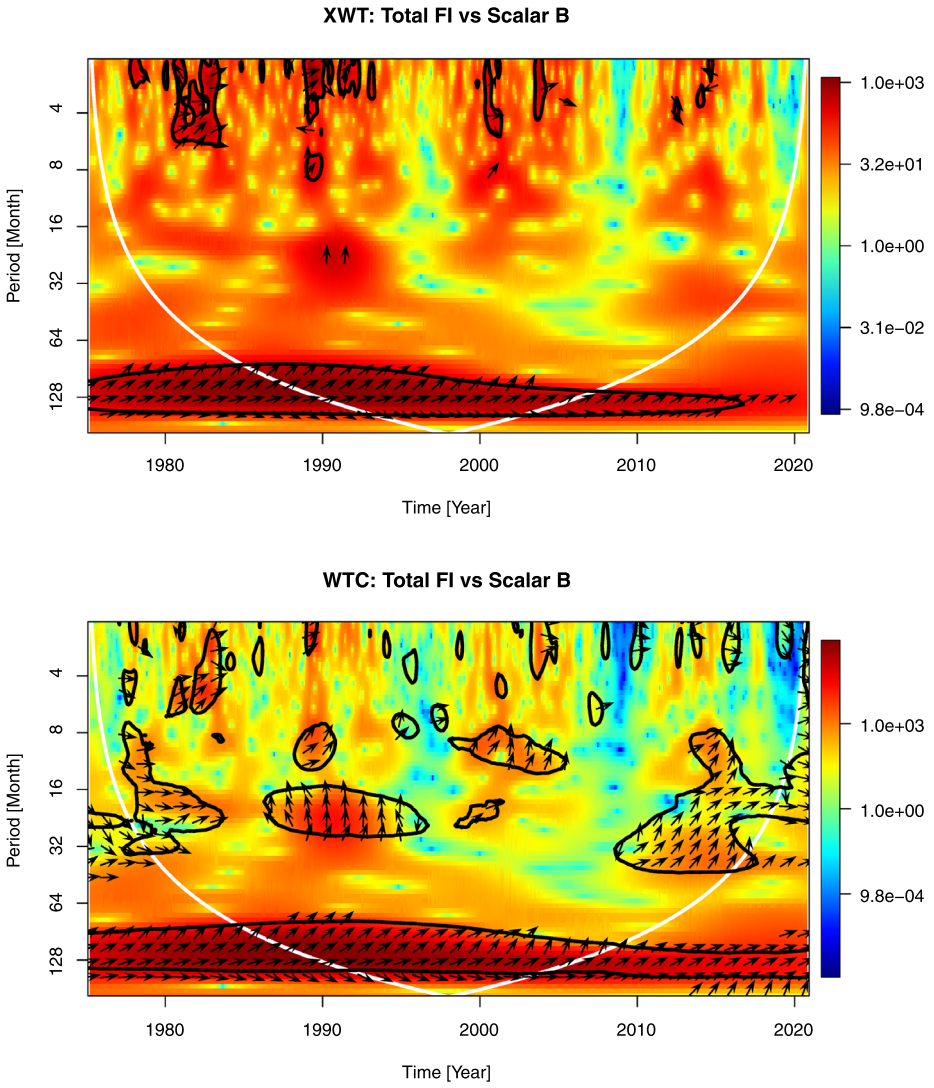

Figure 11 XWT (upper panel) and WTC (lower panel) spectrum between FI and scalar B.

Souza Franco et al. (2021) we found the same periodicity in the same data sets that they analyzed and we further detected this periodicity in the aa data set.

Recently, Ozguc et al. (2021) analyzed the periodic variations of hemispheric and total solar FI data separately for the last solar cycle (Cycle 24) by using the XWT and WTC analyses methods. They compared total FI with hemispheric FI data sets and found strong phase mixing between the Northern and Southern Hemisphere FI data especially for the short periods, while for the long periods they obtained phase coherency between the used data sets. Also, they could not find significant correlation in the case of the Northern and Southern Hemisphere FI data sets, but they obtained a strong correlation between the total FI and Southern Hemisphere data sets. Here, the relative phase difference between the solar

FI and other parameters (aa, Ap, Dst, and scalar B) has been explored using the XWT analysis method. For all parameters, the arrows in small periods (0 – 8 months) are randomly distributed, showing a strong phase mixing (see upper panels in Figures 8 to 11). The arrows in midperiods (8 – 64 months) are directed toward right-up/left-down (aa, Ap, scalar B / Dst) and this indicates that the second variables (aa, Ap, Dst, and scalar B) are leading. The arrows in high periods (around 11 years) were directed toward left/right that shows two variables are in phase (FI and aa, Ap, and scalar B) /antiphase (FI and Dst). The WTC analysis results between monthly solar FI and geomagnetic-activity parameters (aa, Ap, Dst, and scalar B) used in this study show weak correlation for the short-term periods (0 – 8 months) during the investigated time period except during the declining phase of Solar Cycle 23 (see lower panels in Figures 8 to 11). These periods show high coherency during the declining phase of Solar Cycle 23. This result may indicate that the geoeffective solar event increased at that time period compared to others. For the midterm periods (8 – 64 months) the coherencies between the periodicities of the investigated parameters are generally increased. Our findings support the above results and further we may speculate that those periods appearing in geomagnetic activity generally originate from the solar activity, especially during Solar Cycles 21 and 22. Finally, the source of the 11-year periodicity appearing in geomagnetic parameters used in this study is the solar-cyclic variation.

5. Conclusions

In this study, we analyzed the relationship between FI and selected geomagnetic-activity parameters (aa, Ap, Dst, and scalar B) over four decades, 1976 – 2020 (four full solar cycles), on both global and regional scales. We focused on the temporal evolution of the employed solar FI and geomagnetic-activity parameters and quantified the correlation between them. Furthermore, MTM, Morlet wavelet, XWT, and WTC analysis techniques were used for the periodicity analyses of the investigated data sets. The results of our analysis are the following:

- The temporal variations of the used data sets show some differences; all data sets except FI peak values gradually decreased after 1992; the FI data peak value gradually decreased since 1982 (see Figure 1 and Table 1).
- All data sets show double or multiple peaks during the maximum phase of the investigated solar-cycle maxima.
- FI shows the highest correlation with scalar B ($r = 0.69 \pm 0.05$), while it shows the lowest correlation with the Dst index ($r = -0.45 \pm 0.07$) with zero-time lag. Only the geomagnetic aa index shows about a 27-month time lag with the FI data set.
- About 11-year sunspot cycle periodicity and periodicities lower than 3.9 months are observed in all data sets without any exception. All periodicities were observed during the maximum phases of the Solar Cycles 21 – 23, while only a few periodicities were observed during Solar Cycle 24.
- FI data have one special period interval (4.8 – 5.2 months) in which all other parameters do not show this periodicity, while geomagnetic aa, Ap, and Dst indices show 6 – 6.1-month periodicity and this period does not appear in the scalar B and FI data sets.
- Geomagnetic aa and Ap indices have a coincident periodic behavior, while other data sets show some discrepancies.
- XWT spectra between FI and other parameters generally show phase mixing in the small periods (2 – 8 months), while all parameters used in this study are inphase and highly

correlated for the 11-year solar-activity periodicity. Note that FI and Dst index data are in antiphase for the 11-year solar-cycle periodicity.

- In the WTC spectra, correlations are seriously decreasing for small periods for all data sets except for the declining phase of Solar Cycle 23. During this phase of Cycle 23 correlations between small periods seriously increased. Contrary to small periods, correlations for the 8- to 45-month periodicities increased during the investigated time interval (see lower panels of Figures 8 to 11).

Acknowledgments The authors thank the reviewers for their constructive comments and suggestions that significantly improved the manuscript.

Funding V.Y. acknowledges support from NSF AST-1614457, AGS-1954737, AST-2108235, AFOSR FA9550-19-1-0040, NASA 80NSSC17K0016, 80NSSC19K0257, and 80NSSC20K0025 grants

Data Availability Ap, Dst, and scalar B data sets used in this study are downloaded from the OMNIWeb (https://omniweb.gsfc.nasa.gov). The aa index data are taken from the International Service of Geomagnetic Indices (ISGI) website (http://isgi.unistra.fr). The solar-flare index data are taken from the Bogazici University, Kandilli Observatory website (https://astronomi.boun.edu.tr/flare-index).

Declarations

Disclosure of Potential Conflicts of Interest The authors declare that they have no conflicts of interest.

References

Abramenko, V.I.: 2005, Relationship between magnetic power spectrum and flare productivity in solar active regions. *Astrophys. J.* **629**, 1141. DOI.

Abramenko, V., Yurchyshyn, V.: 2010, Magnetic energy spectra in solar active regions. *Astrophys. J.* **720**, 717. DOI.

Ahluwalia, H.S.: 2000, Ap time variations and interplanetary magnetic field intensity. *J. Geophys. Res.* **105**, 27481. DOI.

Atac, T., Ozguc, A.: 1998, Flare index of solar cycle 22. *Solar Phys.* **180**, 397. DOI.

Atac, T., Ozguc, A.: 2001, Flare index during the rising phase of solar cycle 23. *Solar Phys.* **198**, 399. DOI.

Bai, T.: 2003, Periodicities in solar flare occurrence: analysis of cycles 19 – 23. *Astrophys. J.* **591**, 406. DOI.

Bai, T., Sturrock, P.: 1987, The 152-day periodicity of the solar flare occurrence rate. *Nature* **327**, 601. DOI.

Barbieri, L.P., Mahmot, R.E.: 2004, October – November 2003's space weather and operations lessons learned. *Space Weather* **2**, S09002. DOI.

Bartels, J., Heck, N.H., Johnston, H.F.: 1939, The three-hour-range index measuring geomagnetic activity. *J. Geophys. Res.* **44**, 411. DOI.

Cadavid, A.C., Lawrence, J.K., McDonald, D.P., Ruzmaikin, A.: 2005, Independent global modes of solar magnetic field fluctuations. *Solar Phys.* **226**, 359. DOI.

Carrasco, V.M.S., Vaquero, J.M., Gallego, M.C., Sánchez-Bajo, F.: 2016, A normalized sunspot-area series starting in 1832: an update. *Solar Phys.* **291**, 2931. DOI.

Chang, C., Glover, G.H.: 2010, Time-frequency dynamics of resting-state brain connectivity measured with fMRI. *NeuroImage* **50**, 81. DOI.

Chowdhury, P., Choudhary, D.P., Gosain, S., Moon, Y.J.: 2015, Short-term periodicities in interplanetary, geomagnetic and solar phenomena during solar cycle 24. *Astrophys. Space Sci.* **356**, 7. DOI.

Chowdhury, P., Gokhale, M.H., Singh, J., Moon, Y.J.: 2016, Mid-term quasi-periodicities in the CaII-K plage index of the Sun and their implications. *Astrophys. Space Sci.* **361**, 54. DOI.

Chowdhury, P., Kilcik, A., Yurchyshyn, V., Obridko, V.N., Rozelot, J.P.: 2019, Analysis of the hemispheric sunspot number time series for the solar cycles 18 to 24. *Solar Phys.* **294**, 142. DOI.

Dennis, B.R.: 1985, Solar hard X-ray bursts. *Solar Phys.* **100**, 465. DOI.

Droege, W., Gibbs, K., Grunsfeld, J.M., Meyer, P., Newport, B.J., Evenson, P., Moses, D.: 1990, A 153 day periodicity in the occurrence of solar flares producing energetic interplanetary electrons. *Astrophys. J. Suppl.* **73**, 279. DOI.

Du, Z.L.: 2015, Bimodal structure of the solar cycle. *Astrophys. J.* **803**, 15.

Echer, E., Gonzalez, W.D., Gonzalez, A.L.C., Prestes, A., Vieira, L.E.A., dal Lago, A., Guarnieri, F.L., Schuch, N.J.: 2004, Long-term correlation between solar and geomagnetic activity. *J. Atmos. Solar-Terr. Phys.* **66**, 1019. DOI.
Ermolli, I., Giorgi, F., Romano, P., Zuccarello, F., Criscuoli, S., Stangalini, M.: 2014, Fractal and multifractal properties of active regions as flare precursors: a case study based on SOHO/MDI and SDO/HMI observations. *Solar Phys.* **289**, 2525. DOI.
Escudier, R., Mignot, J., Swingedouw, D.: 2013, A 20-year coupled ocean-sea ice-atmosphere variability mode in the North Atlantic in an AOGCM. *Clim. Dyn.* **40**, 619. DOI.
Fang, K., Gou, X., Chen, F., Liu, C., Davi, N., Li, J., Zhao, Z., Li, Y.: 2012, Tree-ring based reconstruction of drought variability (1615 – 2009) in the Kongtong Mountain area, northern China. *Glob. Planet. Change* **80**, 190. DOI.
Feminella, F., Storini, M.: 1997, Large-scale dynamical phenomena during solar activity cycles. *Astron. Astrophys.* **322**, 311.
Ghil, M., Allen, M.R., Dettinger, M.D., Ide, K., Kondrashov, D., Mann, M.E., Robertson, A.W., Saunders, A., Tian, Y., Varadi, F., Yiou, P.: 2002, Advanced spectral methods for climatic time series. *Rev. Geophys.* **40**, 1003. DOI.
Gnevyshev, M.N.: 1967, On the 11-years cycle of solar activity. *Solar Phys.* **1**, 107. DOI.
Gnevyshev, M.N.: 1977, Essential features of the 11-year solar cycle. *Solar Phys.* **51**, 175. DOI.
Gonzalez, W.D., Gonzalez, A.L.C., Tsurutani, B.T.: 1990, Dual-peak solar cycle distribution of intense geomagnetic storms. *Planet. Space Sci.* **38**, 181. DOI.
Gonzalez, W.D., Tsurutani, B.T., Clúa de Gonzalez, A.L.: 1999, Interplanetary origin of geomagnetic storms. *Space Sci. Rev.* **88**, 529. DOI.
Grinsted, A., Moore, J.C., Jevrejeva, S.: 2004, Application of the cross wavelet transform and wavelet coherence to geophysical time series. *Nonlinear Process. Geophys.* **11**, 561. DOI.
Ichimoto, K., Kubota, J., Suzuki, M., Tohmura, I., Kurokawa, H.: 1985, Periodic behaviour of solar flare activity. *Nature* **316**, 422. DOI.
Kakad, B., Kakad, A., Ramesh, D.S., Lakhina, G.S.: 2019, Diminishing activity of recent solar cycles (22 – 24) and their impact on geospace. *J. Space Weather Space Clim.* **9**, A1. DOI.
Kane, R.P.: 2010, Gnevyshev peaks in geomagnetic indices. *Planet. Space Sci.* **58**, 749. DOI.
Kilcik, A., Ozguc, A., Rozelot, J.P., Atac, T.: 2010, Periodicities in solar flare index for cycles 21 – 23 revisited. *Solar Phys.* **264**, 255. DOI.
Kilcik, A., Yurchyshyn, V.B., Abramenko, V., Goode, P.R., Gopalswamy, N., Ozguc, A., Rozelot, J.P.: 2011, Maximum coronal mass ejection speed as an indicator of solar and geomagnetic activities. *Astrophys. J.* **727**, 44. DOI.
Kilcik, A., Yiğit, E., Yurchyshyn, V., Ozguc, A., Rozelot, J.P.: 2017, Solar and geomagnetic activity relation for the last two solar cycles. *Sun Geosph.* **12**, 31.
Kilcik, A., Yurchyshyn, V., Donmez, B., Obridko, V.N., Ozguc, A., Rozelot, J.P.: 2018, Temporal and periodic variations of sunspot counts in flaring and non-flaring active regions. *Solar Phys.* **293**, 63. DOI.
Kilcik, A., Chowdhury, P., Sarp, V., Yurchyshyn, V., Donmez, B., Rozelot, J.-P., Ozguc, A.: 2020, Temporal and periodic variation of the MCMESI for the last two solar cycles; comparison with the number of different class X-ray solar flares. *Solar Phys.* **295**, 159. DOI.
Kile, J.N., Cliver, E.V.: 1991, A search for the 154 day periodicity in the occurrence rate of solar flares using Ottawa 2.8 GHz burst data, 1955 – 1990. *Astrophys. J.* **370**, 442. DOI.
Kilpua, E.K.J., Luhmann, J.G., Jian, L.K., Russell, C.T., Li, Y.: 2014, Why have geomagnetic storms been so weak during the recent solar minimum and the rising phase of cycle 24? *J. Atmos. Solar-Terr. Phys.* **107**, 12. DOI.
Kirov, B., Asenovski, S., Georgieva, K., Obridko, V.N., Maris-Muntean, G.: 2018, Forecasting the sunspot maximum through an analysis of geomagnetic activity. *J. Atmos. Solar-Terr. Phys.* **176**, 42. DOI.
Kleczek, J.: 1952, Catalogue de l'activite des Ã©ruptions chromosphériques. Premiere partie. *Publ. No. - Astron. Inst. Czechoslov. Acad. Sci.* **22**, 1.
Knaack, R., Stenflo, J.O., Berdyugina, S.V.: 2005, Evolution and rotation of large-scale photospheric magnetic fields of the Sun during cycles 21 – 23. Periodicities, north-south asymmetries and r-mode signatures. *Astron. Astrophys.* **438**, 1067. DOI.
Knoska, S., Petrasek, J.: 1984, Chromospheric flare activity in SOLAR-CYCLE-20. *Contrib. Astron. Obs. Skaln. Pleso* **12**, 165.
Maraun, D., Kurths, J.: 2004, Cross wavelet analysis: significance testing and pitfalls. *Nonlinear Process. Geophys.* **11**, 505. DOI.
Mares, I., Dobrica, V., Mares, C., Demetrescu, C.: 2021, Assessing the solar variability signature in climate variables by information theory and wavelet coherence. *Sci. Rep.* **11**, 11337. DOI.
Marques de Souza Franco, A., Hajra, R., Echer, E., Bolzan, M.J.A.: 2021, Seasonal features of geomagnetic activity: a study on the solar activity dependence. *Ann. Geophys.* **39**, 929. DOI. https://angeo.copernicus.org/articles/39/929/2021/.

Mayaud, P.-N.: 1972, The aa indices: a 100-year series characterizing the magnetic activity. *J. Geophys. Res.* **77**, 6870. DOI.
Oloketuyi, J., Liu, Y., Zhao, M.: 2019, The periodic and temporal behaviors of solar X-ray flares in solar cycles 23 and 24. *Astrophys. J.* **874**, 20. DOI.
Owens, M.J., Forsyth, R.J.: 2013, The heliospheric magnetic field. *Living Rev. Solar Phys.* **10**, 5. DOI.
Ozguc, A., Atac, T.: 1989, Periodic behavior of solar flare index during solar cycles 20 and 21. *Solar Phys.* **123**, 357. DOI.
Ozguc, A., Kilcik, A., Sarp, V., Yesilyaprak, H., Pektas, R.: 2021, Periodic variation of solar flare index for the last solar cycle (Cycle 24). *Adv. Astron.* **2021**, 5391091. DOI.
Park, J.: 1992, *Envelope Estimation for Quasi-Periodic Geophysical Signals in Noise: A Multitaper Approach, in Statistics in the Environmental and Earth Sciences*, Edward Arnold, London, 189.
Percival, D.B., Walden, A.T.: 1993, *Spectral Analysis for Physical Applications*, Cambridge University Press, Cambridge. DOI. ISBN 978-0521435413.
Poluianov, S., Usoskin, I.: 2014, Critical analysis of a hypothesis of the planetary tidal influence on solar activity. *Solar Phys.* **289**, 2333. DOI.
Rieger, E., Kanbach, G., Reppin, C., Share, G.H., Forrest, D.J., Chupp, E.L.: 1984, A 154-day periodicity in the occurrence of hard solar flares? *Nature* **312**, 623. DOI.
Singh, Y.P., Badruddin: 2014, Prominent short-, mid-, and long-term periodicities in solar and geomagnetic activity: wavelet analysis. *Planet. Space Sci.* **96**, 120. DOI.
Storini, M., Bazilevskaya, G.A., Fluckiger, E.O., Krainev, M.B., Makhmutov, V.S., Sladkova, A.I.: 2003, The GNEVYSHEV gap: a review for space weather. *Adv. Space Res.* **31**, 895. DOI.
Sugiura, M.: 1964, Hourly values of equatorial Dst for the IGY. *Ann. Int. Geophys. Year* **35**, 9.
Takalo, J.: 2021, Comparison of geomagnetic indices during even and odd solar cycles SC17 – SC24: signatures of Gnevyshev gap in geomagnetic activity. *Solar Phys.* **296**, 19. DOI.
Thomson, D.J.: 1982, Spectrum estimation and harmonic analysis. *Proc. IEEE* **70**, 1055.
Torrence, C., Compo, G.P.: 1998, A practical guide to wavelet analysis. *Bull. Am. Meteorol. Soc.* **79**, 61.
Vaquero, J.M., Gallego, M.C., Trigo, R.M.: 2007, Sunspot numbers during 1736 – 1739 revisited. *Adv. Space Res.* **40**, 1895. DOI.
Verbanac, G., Mandea, M., Vršnak, B., Sentic, S.: 2011, Evolution of solar and geomagnetic activity indices, and their relationship: 1960 – 2001. *Solar Phys.* **271**, 183. DOI.
Verma, V.K., Joshi, G.C., Uddin, W., Paliwal, D.C.: 1991, Search for a 152 – 158 days periodicity in the occurrence rate of solar flares inferred from spectral data of radio bursts. *Astron. Astrophys. Suppl. Ser.* **90**, 83.
Xiang, N.B., Kong, D.F.: 2015, What causes the inter-solar-cycle variation of total solar irradiance? *Astron. J.* **150**, 171. DOI.